Residential Photovoltaic and Battery Energy System with Grid Support Functionalities

Iromi Ranaweera, Santiago Sanchez, Ole-Morten Midtgård
Department of Electric Power Engineering, Norwegian University of Science and Technology
7491 Trondheim, Norway
Email: iromi.ranaweera@ntnu.no

***Abstract*—This paper presents the design of a control system for a grid connected residential photovoltaic (PV) system with battery energy storage (BES). The control methods for the power electronic converters are presented and the potential of utilizing BES for participating in primary frequency regulation of the grid is investigated. The charging/ discharging rate of the battery is controlled based on the frequency droop characteristic. The performance of the control system is validated in a simulation study, in which fast response and perfect tracking of the set points are observed in (i) normal operating condition and (ii) a case where the grid frequency varies. The amount of the battery's capacity that can be utilized for this purpose depends on the quantity of power generated by the PV system, as well as the load level. The study shows that sometimes the rated capacity of the battery could be fully utilized for serving the primary frequency regulation purposes.**

I. Introduction

The decline in PV module prices accompanied by financial incentives, such as feed in tariffs, as well as increased price of electricity, have caused a rapid increase in grid connected residential photovoltaic systems around the world. The increase in the adoption of distributed generation (DG) in the low voltage network creates several technical challenges such as voltage rise, voltage fluctuations, current harmonics and DC current injection by the connected inverters, and unintentional islanding [1]–[3]. One of the major technical issues which has received much attention among these, is the over-voltage problem caused by reverse power flow. Reactive power absorption by PV inverters and active power curtailments have been suggested and are already implemented in grid codes to deal with this issue [4], [5]. Initially, relatively high feed in tariff (FIT) rates compared to the utility electricity prices were paid in order to promote PV systems at the residential level. However, over time a decrease in FIT has been observed [6], which encourage customers to increase self consumption. The increase in self-consumption can be achieved by either demand side management or energy storage solutions (ESSs). The need for more energy storage in the grid also arises due to the general increase in renewable generators. As the number of such generators becomes significant, the difficulty of maintaining grid stability increases. This is mainly caused by the uncontrollable and intermittent nature of their power output. Hence, the grid requires ESSs for compensating the generation fluctuations caused by renewable sources. There are several potential applications of storage both in the residential scale and the utility scale, such as load leveling, peak shaving, capacity firming, spinning reserve and ancillary services such as frequency regulation, power quality improvement and voltage support.

In this paper we investigate the potential of utilizing residential PV systems with BES for primary frequency regulation of the grid. The following section describes the configuration of the system. The section III presents modelling and design of controllers for the converters. Section IV describes the power management system which includes the primary frequency regulation. Finally results of the simulation study are provided with the conclusion.

II. System Configuration

The configuration of the residential PV system with BES is illustrated in Fig. 1. A DC-DC converter is adopted to control the output voltage of the PV array. The battery bank is connected to the stable DC link via a bi-directional DC-DC converter which controls the power transfer from/to the battery. The system is connected to the grid and the local load via a single phase DC-AC bi-directional converter (grid converter). The grid converter maintains the DC link voltage at a constant level and controls the active and reactive power exchange with the grid and the local system.

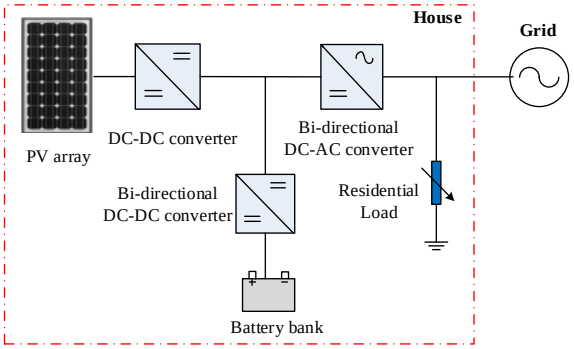

Fig. 1: Configuration of the residential PV system with BES.

III. Modelling and Control Design

A. PV Array

The relation between the output voltage (v_{pv}) and the current (i_{pv}) of a PV module based on the single diode equivalent model is

$$i_{pv} = I_{ph} - I_o\left(exp\left(\frac{q(v_{pv}+i_{pv}R_s)}{akTn_s}\right)-1\right)-\frac{v_{pv}+i_{pv}R_s}{R_{sh}}, \quad (1)$$

where I_{ph} is the photon generated current, I_o is the diode saturation current, R_s is the series resistance of the module, R_{sh} is the shunt resistance of the module, n_s is the number of series connected cells per module, a is the diode ideality factor, T is the module temperature (K), q is the charge of an electron (1.602×10^{-19} C) and k is the Boltzmann constant (1.3806×10^{-23} J/K).

The photon generated current depends on the irradiance (G) and the operating temperature of the PV module.

$$I_{ph} = \frac{G}{G_{STC}}\Big(I_{ph,STC} + K_i(T - T_{STC})\Big) \tag{2}$$

The diode saturation current depends on the module temperature,

$$I_o = \frac{I_{ph,STC} + K_i(T - T_{STC})}{exp\left(\frac{q\left(V_{oc,STC} + K_v(T - T_{STC})\right)}{akTn_s}\right) - 1}\,, \tag{3}$$

where subscript STC denotes the parameter values at standard test conditions (1000 W/m^2, 25 °C). K_i is the current temperature coefficient and K_v is the voltage temperature coefficient of the PV module.

Assuming all the PV modules in the PV array are uniformly illuminated, the mathematical model of the PV module can be extended for a PV array as follows.

$$i_{pv} = N_p I_{ph} - N_p I_o\left(exp\left(\frac{q(v_{pv} + i_{pv}R_s\frac{N_s}{N_p})}{akTn_sN_s}\right) - 1\right) - \frac{v_{pv} + i_{pv}R_s\frac{N_s}{N_p}}{R_{sh}\frac{N_s}{N_p}} \tag{4}$$

N_s is the number of modules connected in series and N_p is the number of strings connected in parallel in the PV array.

A model of a PV array with rated capacity of 4 kWp is built in Matlab/Simulink with the parameters listed in Table I. The I-V characteristic of the PV array is shown in Fig. 2.

TABLE I: PV array parameters.

Parameter	Value	Parameter	Value
R_s	0.094 Ω	$I_{ph,STC}$	8.878 A
R_{sh}	3545.09 Ω	K_i	0.065 %/°C
a	1.75	K_v	-0.35 %/°C
n_s	72	N_s	7
$V_{oc,STC}$	44.6 V	N_p	2

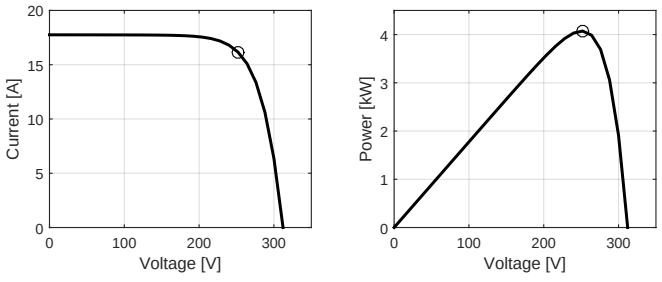

Fig. 2: I-V characteristic of the PV array at STC.

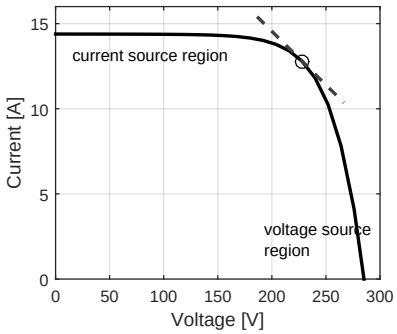

Fig. 3: Linearization of I-V characteristic about MPP at nominal operating condition.

B. Battery

The dynamic model of a Li-ion battery presented in [7] is used in this work. The parameters of the battery are listed in Table II.

TABLE II: Battery parameters.

Parameter	Value
Rated capacity	140 Ah
Nominal voltage	48 V
Fully charged volttage	55.87 V
Nominal discharge current	60.87 A
Internal resistance	0.0034 Ω

C. Boost converter

The I-V characteristic of a PV array is non-linear and changes with the irradiance and the ambient temperature. This non-linear behaviour causes variations in the power output of the PV array, resulting in a peak at a specific voltage and current which is known as the maximum power point (MPP). The MPP voltage changes as the irradiance and the module temperature changes. In order to extract the maximum power from the PV array, the output voltage of the array should be maintained at the MPP voltage. In this system, the PV array's output voltage is regulated by controlling the input voltage of the boost converter. The voltage controller maintains the input voltage of the boost converter at the reference value generated by the maximum power point tracking (MPPT) algorithm. The MPPT algorithm is developed based on the incremental conductance method [8], [9].

The average model of the boost converter

$$\begin{aligned} L_b\dot{i}_{L,b} &= v_{pv} - (1-d)V_{dc} \\ C_1\dot{v}_{pv} &= \frac{V_{eq} - v_{pv}}{R_{eq}} - i_{L,b} \end{aligned} \tag{5}$$

V_{eq} and R_{eq} are the equivalent voltage and the dynamic equivalent resistance of the PV array derived by linearizing the non-linear model of the PV array about the MPP operating point at the nominal operating condition (800 W/m^2, ambient temperature 20°C) as described in [10], and d is the duty ratio. The rest of the notations are with reference to Fig. 6. The equivalent resistance corresponds to $-\frac{dv_{pv}}{di_{pv}}$ of the PV array's IV characteristic at MPP at nominal operating conditions. The

dynamic resistance $\left(-\frac{dv_{pv}}{di_{pv}}\right)$ gradually increases from the open circuit point towards MPP and then rapidly changes when moving away from the constant voltage region and held almost constant in the current source region.

The small signal model of the boost converter is derived from perturbation and linearization about the steady state operating point, $d = D, v_{pv} = V_{pv}, i_{L,b} = I_{L,b}$.
Introducing perturbations

$$\begin{aligned} d &= D - \tilde{d} \\ v_{pv} &= V_{pv} + \tilde{v}_{pv} \\ i_{L,b} &= I_{L,b} + \tilde{i}_{L,b} \end{aligned} \tag{6}$$

Substituting Eq.(6) into Eq.(5) and neglecting the higher order terms the following small signal model is obtained.

$$\begin{aligned} L_b \dot{\tilde{i}}_{L,b} &= \tilde{v}_{pv} - \tilde{d} V_{dc} \\ C_1 \dot{\tilde{v}}_{pv} &= -\frac{\tilde{v}_{pv}}{R_{eq}} - \tilde{i}_{L,b} \end{aligned} \tag{7}$$

Applying Laplace transformation to Eq.(7), the small signal transfer function from the duty ratio to the input voltage can be obtained.

$$\frac{V_{pv}(s)}{d(s)} = \frac{V_{dc}}{1 + \frac{L_b}{R_{eq}} s + L_b C_1 s^2} \tag{8}$$

The transfer function is a second-order system with, $\omega_n = \frac{1}{\sqrt{L_b C_1}}$ and $\xi = \frac{1}{2R_{eq}} \sqrt{\frac{L_b}{C_1}}$. The boost converter is designed with input voltage range 120−300 V, switching frequency 10 kHz, L_b = 10 mH and C_1 = 47 μF. The DC link voltage is 400 V. Fig. 4 shows the bode plots of the transfer function in Eq. (8) for three different R_{eq} at different operating points on the curve in Fig. 3. $R_{eq} = 150.095\ \Omega$ corresponds to the MPP at nominal operating conditions. From the phase plot it can be observed that the open loop system does not have a sufficient phase margin that can guarantee better performance, hence a PI controller cannot be used for input voltage control. A lead-lag compensator that can provide sufficient phase margin and high gain at low frequencies is designed to achieve fast response with low overshoot. The controller transfer function is given by

$$G_c(s) = G_{co} \frac{(1 + \frac{s}{\omega_z})(1 + \frac{\omega_L}{s})}{(1 + \frac{s}{\omega_p})} \tag{9}$$

The bode plot of the system before and after compensation with lead-lag compensator is shown in Fig. 5. Since switching frequency is 10 kHz the cross-over frequency is chosen to be 1 kHz. The lead-lag compensator parameters are, $G_{co} = 0.0039$, $\omega_z = 549.71$ rad/s, $\omega_L = 314.16$ rad/s, $\omega_p = 71817$ rad/s.

D. Single-phase DC-AC converter (Grid converter)

Control of the reactive power and the voltage of the DC link is achieved by the grid converter. The current controller for the grid converter is designed in the synchronous reference frame (dq frame). Two orthogonal components are required to transform phase variables into the dq frame variables. As in a single phase system only one phase is available, a fictitious second phase which is orthogonal to the real one is made by delaying the real signal by $\frac{1}{4}$ of the period of the original

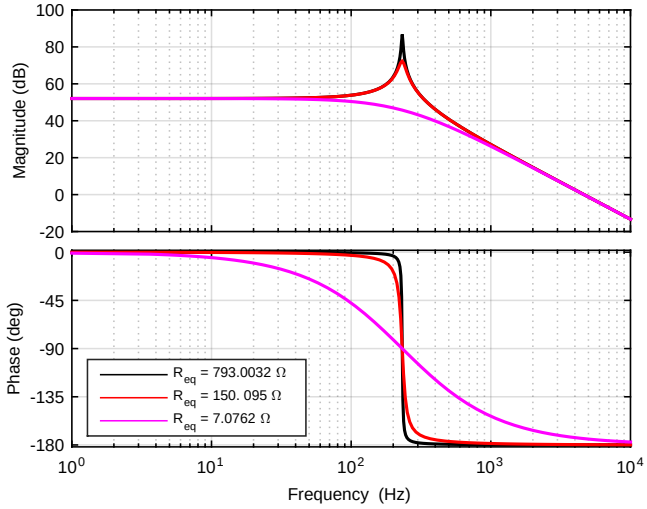

Fig. 4: Bode plots of the system transfer function for different dynamic equivalent resistance.

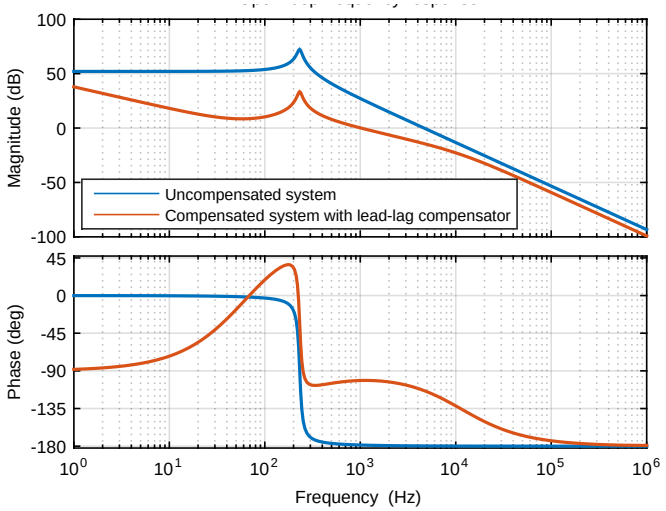

Fig. 5: Bode plots of the system transfer function before and after compensation.

signal. Then the voltage equations in the dq reference frame are

$$\begin{aligned} L_f \frac{di_d}{dt} &= -v_{gd} + \omega L_f i_q - R_f i_d + v_{con,d} \\ L_f \frac{di_q}{dt} &= -v_{gq} - \omega L_f i_d - R_f i_q + v_{con,q} \\ v_{con,d} &= d_d V_{dc}\ , \quad v_{con,q} = d_q V_{dc} \end{aligned} \tag{10}$$

$\omega = 2\pi f$, f is the grid frequency, R_f is the filter resistance and subscripts d and q denote the variables in the dq reference frame.
The transfer function from duty ratio to dq axis currents are

$$\begin{aligned} i_d(s) &= \frac{V_{dc}\ d_d(s)}{R_f + L_f s} - \frac{v_{gd}(s)}{R_f + L_f s} + \frac{\omega L\ i_q(s)}{R_f + L_f s} \\ i_q(s) &= \frac{V_{dc}\ d_q(s)}{R_f + L_f s} - \frac{v_{gq}(s)}{R_f + L_f s} - \frac{\omega L\ i_d(s)}{R_f + L_f s} \end{aligned} \tag{11}$$

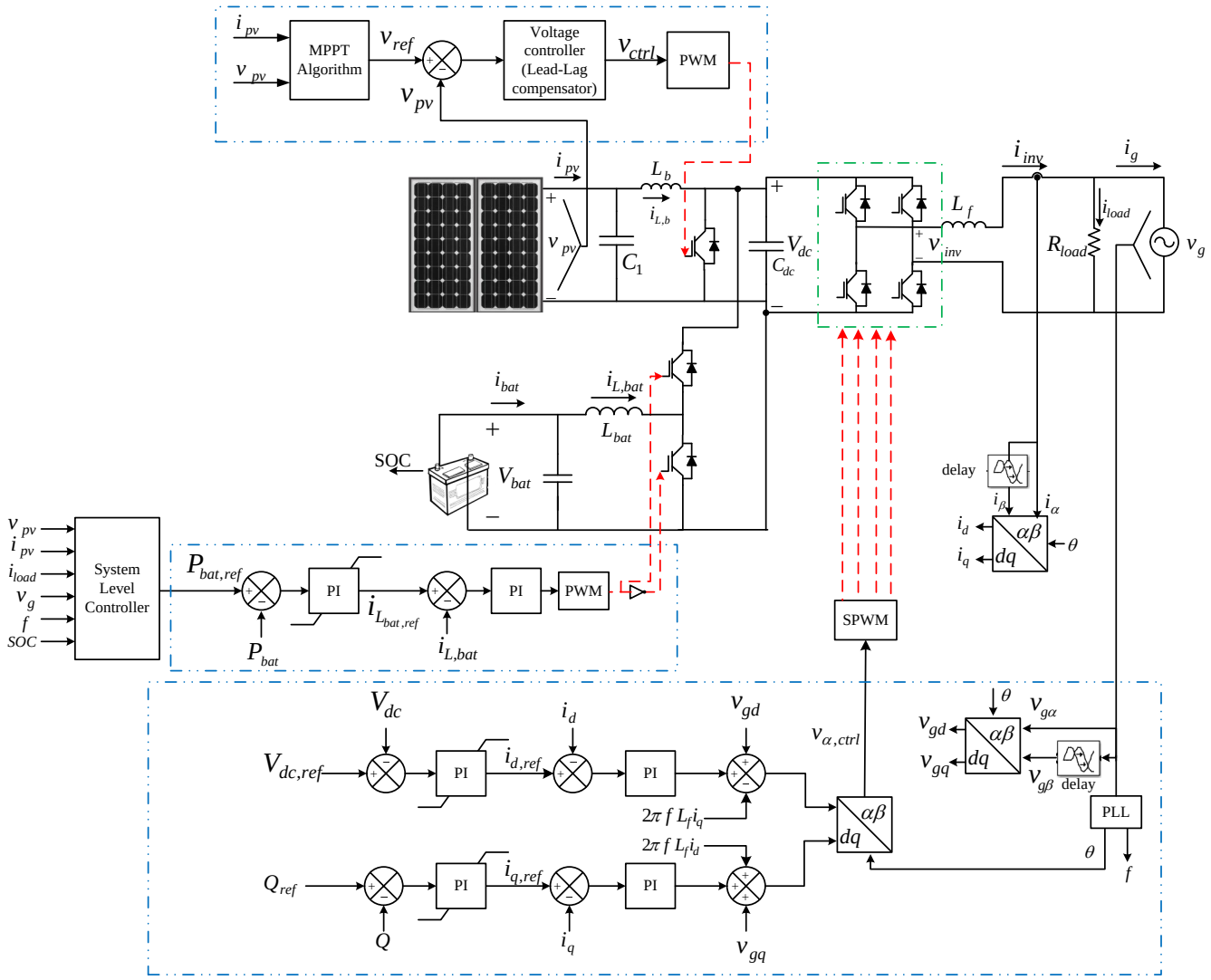

Fig. 6: The system configuration and control overview.

According to the above equations, d and q axis are coupled, hence coupling terms should be compensated in order to achieve independent control of d and q axis. In addition, in order to obtain good dynamic response and grid disturbance rejection, grid voltage feed-forward is used. The controllers are chosen to be PI controllers and tuned using modulus optimum method to achieve optimal performance. The control system of the grid converter with compensation of coupling terms and grid voltage feed forward is shown in Fig. 6. The d-axis reference current is generated by the outer DC link voltage controller and the q-axis reference current is generated by the outer reactive power controller. DC link voltage controller and the outer reactive power controller are also chosen to be PI controllers. The symmetrical optimum method is used to tune the DC link voltage controller.

E. Bidirectional DC-DC converter

The main objectives of the bidirectional converter are to provide the interface between the battery bank and the DC link, which are operating at two voltage levels, and achieve smooth charging/discharging of the battery. The proposed control system for the bidirectional converter is shown in Fig. 6. A PI controller is adopted to control the current through the inductor. The reference value for the current controller is generated by the outer power controller. The power reference for the power controller is generated from the power management system. The voltage of the battery bank is dependent on the state of charge (SOC) of the battery. If the battery continuously receives energy when it is fully charged, then the battery voltage gets too high, resulting in electrolysis of the water and overheating. Fully discharging the battery accelerates the battery's degradation. Hence, the power transfer to the battery should be discontinued when the battery SOC/ voltage reaches the limits. This can be achieved by controlling the power reference in response to the battery voltage/ SOC.

IV. Power Management

The control system of the PV system with battery storage consists of two levels: device level control and system level

coordinated control. The power management system belongs to the system level control. The system level controller generates the power references for the device level controllers. The energy management system, together with the power management system determines the amount of power need to be transferred to the battery and the grid based on energy price, sell back rate, grid feed in limitations, battery state of charge, and several others [11], [12]. From the power balance, power exchanged with the grid in normal operation is

$$P_{grid} = P_{pv} + P_{bat} - P_{load} \,, \tag{12}$$

where P_{grid} is the power exchanged with the grid, P_{pv} is the power output of the PV system, P_{bat} is the battery power and P_{load} is the load. The applied sign convention: $P_{pv} > 0, P_{load} > 0$, Battery discharging: $P_{bat} > 0$, Power injection to the grid: $P_{grid} > 0$.

A. Primary Frequency Regulation

The mismatch in load and generation creates changes in the grid frequency. In order to restore the grid frequency, first fast reacting primary reserves are brought on-line in response to the grid frequency changes called primary frequency regulation. Then the slower responding reserves brought on-line to bring the frequency back to the nominal value, which is known as secondary frequency regulation. If the frequency imbalance lasts for long, sometimes tertiary reserves are used. Recently there has been a growing interest in using grid scale BES for primary frequency regulation. Meanwhile, growing demand for residential level BES especially coupled with PV systems can be observed. There is a potential of using these small systems for primary frequency regulations. Even though the individual contribution is not that significant, the cumulative effect of many systems become significant when the number of systems connected to the grid become larger. Hence, it is worth it to investigate the capability of such systems in participating primary frequency regulation.

Primary frequency reserves should respond relatively fast (a few seconds and below) for grid frequency changes [13]. As the batteries can respond relatively fast they are a good source of primary frequency regulation. The BES in a residential system like the one shown in Fig. 1, should decrease discharging rate or increase charging rate depending on the operation of the battery when grid frequency goes up. Alternatively, the discharging rate of the battery should increase or charging rate should decrease when the grid frequency goes down. The available power capacity of the battery is more important than the available energy capacity in primary frequency regulation applications, because primary reserves are used only for a short time, thus there is no requirement of higher energy capacity.

Assuming the rated capacity of the battery is available for primary frequency regulation, Power vs frequency characteristic can be defined as shown in Fig. 7. In the figure, P_{freq} is the battery power capacity participating in primary frequency regulation, $P_{bat,rate}$ is the rated charge/discharge capacity of the battery and f_{nom} is the nominal grid frequency. Even though it is assumed that the rated battery capacity is available, that is not always true. Therefore the real battery capacity that can be utilized is subjected to the following constraints.
Battery capacity constraint

$$\begin{aligned} -P_{bat,rate} \leq (P_{bat} + P_{freq}) \leq P_{bat,rate} \\ P_{bat,rate} \leq P_{conB,rate} \end{aligned} \tag{13}$$

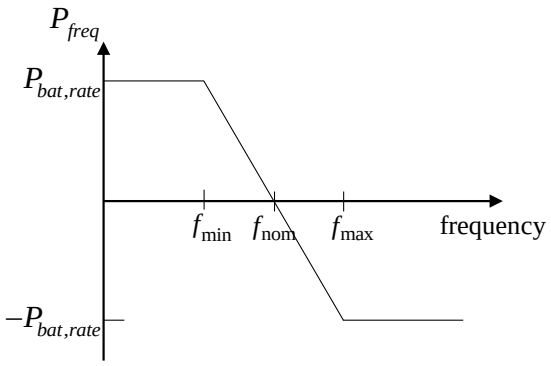

Fig. 7: Power-frequency characteristic.

$P_{conB,rate}$ is the rated capacity of the bi-directional DC-DC converter.
Grid converter capacity constraint

$$-P_{conG,rate} \leq P_{pv} + P_{bat} + P_{freq} \leq P_{conG,rate} \tag{14}$$

$P_{conG,rate} = \sqrt{S_{conG,rate}^2 - Q_{conG}^2}$, where $S_{conG,rate}$ is the kVA rating of the grid converter and Q_{conG} is the reactive power (kVAr) absorbed or supplied by the grid converter. The calculated value from the power-frequency characteristic should satisfy the constraints (13) and (14). If not the maximum possible capacity should be utilized. Because of the constraints, sometimes the effective power capacity of the battery that can be utilized for frequency regulation can be zero.

V. Simulation Results

Simulations are carried out for a PV system with BES for investigating the effectiveness of the control system. The simulation results have been presented for, 1) normal operation and 2) grid frequency variation. Fig. 8 presents a summary of the key results for normal operation of the system. In order to test the robustness of the overall control system for disturbances (variation of irradiance and load) step changes in irradiance at $t = [0.75\ 1.75]$ s and the load at $t = 2.5$ s are applied. As shown in the results, incremental conductance algorithm, along with the input voltage controller of the boost converter, is able to track the MPP effectively when irradiance changes. The sampling time of the MPPT algorithm is 5 ms with voltage change of 0.5 V per sampling interval. The DC link voltage controller is able to maintain stable DC link voltage with negligible overshoot during disturbances. Current controller of the battery converter responds instantaneously to the changes with zero over shoot. Fig. 9 shows the power sharing between the components. Smooth power transfer among the system components is achieved, ensuring the effectiveness of both device level and system level controllers. At time $t = 1.2$ s the reactive power reference is changed from 0 to 1000 VAr, and the reactive power controller tracks the reference with negligible overshoot. The bi-directional battery current and power controllers show optimal performance with no overshoot and fast response time.

The rated capacity of the battery converter used in the system is 3 kW while grid converter's rated capacity is 4 kW.

The rated discharging capacity of the battery is determined by the battery converter's rated capacity. The slope of the frequency characteristic is chosen to be 3.75 kW/Hz and $f = 50$ Hz, $f_{min} = 49.2$ Hz, $f_{max} = 50.8$ Hz. The simulation results of the system responses for grid frequency changes are shown in Fig. 10 and Fig. 11. Initially the power production from the PV array is almost zero, hence the residential load is supplied by the grid and battery stays idle. At $t = 0.5$ s the grid frequency deviates from the nominal frequency of 50 Hz. The battery starts to charge from the grid as the grid frequency increases and charging rate gradually increases, analogous to the grid frequency. The battery reaches its rated charging rate of 3 kW when the grid frequency goes to 50.8 Hz. At $t = 0.75$ s power production from the PV system increases and this power is transferred to the battery. The load is still supplied by the grid. At $t = 1$ s the grid frequency starts to gradually decrease, hence the battery charging rate decreases correspondingly and the PV system starts to supply the load. Alternatively, when the grid frequency decreases from 50 Hz, the battery starts to discharge correspondingly to the grid frequency and reaches rated discharging rate when the grid frequency goes down to 49.2 Hz. When the power production from the PV system increases at $t = 0.75$ s, battery charging rate drops and the PV system starts to supply the local load while injecting excess power to the grid by utilizing the rated capacity of the grid converter. When the system frequency is restored the system returns to the normal operation supplying the load from the PV array and transferring the excess power to the battery, assuming SOC of the battery is lower than the maximum SOC.

VI. Conclusion

The control scheme for the PV system with BES connected to the grid through a single phase DC-AC converter is presented with the simulation results. The potential of participating this system in primary frequency regulation is investigated. The optimal performance of the controllers with low overshoot and fast response time are achieved for various operating conditions by proper tuning. Fast responses of the battery for grid frequency changes are observed according to the frequency droop characteristic. It is found that the potential contribution to the primary frequency regulation of the battery can vary from zero to rated capacity of the battery. The capacity available for this purpose is determined by the power output of the PV array and the load.

References

[1] E. Caamano, J. Thornycroft, and H. Moor, "State of the art on dispersed pv power generation:Publication review on the impacts of pv distributed generation and electricity networks," tech. rep., Intelligent Energy-Europe, 2007.

[2] M. ElNozahy and M. Salama, "Technical impacts of grid-connected photovoltaic systems on electrical networks-A review," *Journal of Renewable ans Sustainable Energy*, vol. 5, May 2013.

[3] M. A. Eltawil and Z. Zhao, "Grid-connected photovoltaic power systems: Technical and potential problemsa review," *Renewable and Sustainable Energy Reviews*, vol. 14, no. 1, pp. 112 – 129, 2010.

[4] B. Craciun, T. Kerekes, D. Sera, and R. Teodorescu, "Overview of recent grid codes for PV power integration," in *International Conference on Optimization of Electrical and Electronic Equipment (OPTIM)*, May 2012.

[5] S. Weckx, C. Gonzalez, and J. Driesen, "Combined central and local active and reactive power control of pv inverters," *Sustainable Energy, IEEE Transactions on*, vol. 5, pp. 776–784, July 2014.

[6] H. Wirth, "Recent facts about photovoltaics in germany," tech. rep., Fraunhofer Institute for Solar Energy Systems ISE, 2014.

[7] O. Tremblay and L.-A. Dessaint, "Experimental validation of a battery dynamic model for EV applications," *World Electric Vehicle Journal*, vol. 3, 2009.

[8] N. A. Kamarzaman and C. W. Tan, "A comprehensive review of maximum power point tracking algorithms for photovoltaic systems," *Renewable and Sustainable Energy Reviews*, vol. 37, no. 0, pp. 585 – 598, 2014.

[9] A. R. Reisi, M. H. Moradi, and S. Jamasb, "Classification and comparison of maximum power point tracking techniques for photovoltaic system: A review," *Renewable and Sustainable Energy Reviews*, vol. 19, no. 0, pp. 433 – 443, 2013.

[10] M. Villalva, T. de Siqueira, and E. Ruppert, "Voltage regulation of photovoltaic arrays: small-signal analysis and control design," *Power Electronics, IET*, vol. 3, pp. 869–880, Nov 2010.

[11] Y. Riffonneau, S. Bacha, F. Barruel, and S. Ploix, "Optimal power flow management for grid connected pv systems with batteries," *IEEE Transactions on Sustainable Energy*, vol. 2, pp. 309–320, July 2011.

[12] E. Ratnam, S. Weller, and C. Kellett, "An optimization-based approach to scheduling residential battery storage with solar pv: Assessing customer benefit," *Renewable Energy*, vol. 75, pp. 123–134, March 2015.

[13] A. Hoke and D. Maksimovic, "Active power control of photovoltaic power systems," in *Technologies for Sustainability (SusTech), 2013 1st IEEE Conference on*, pp. 70–77, Aug 2013.

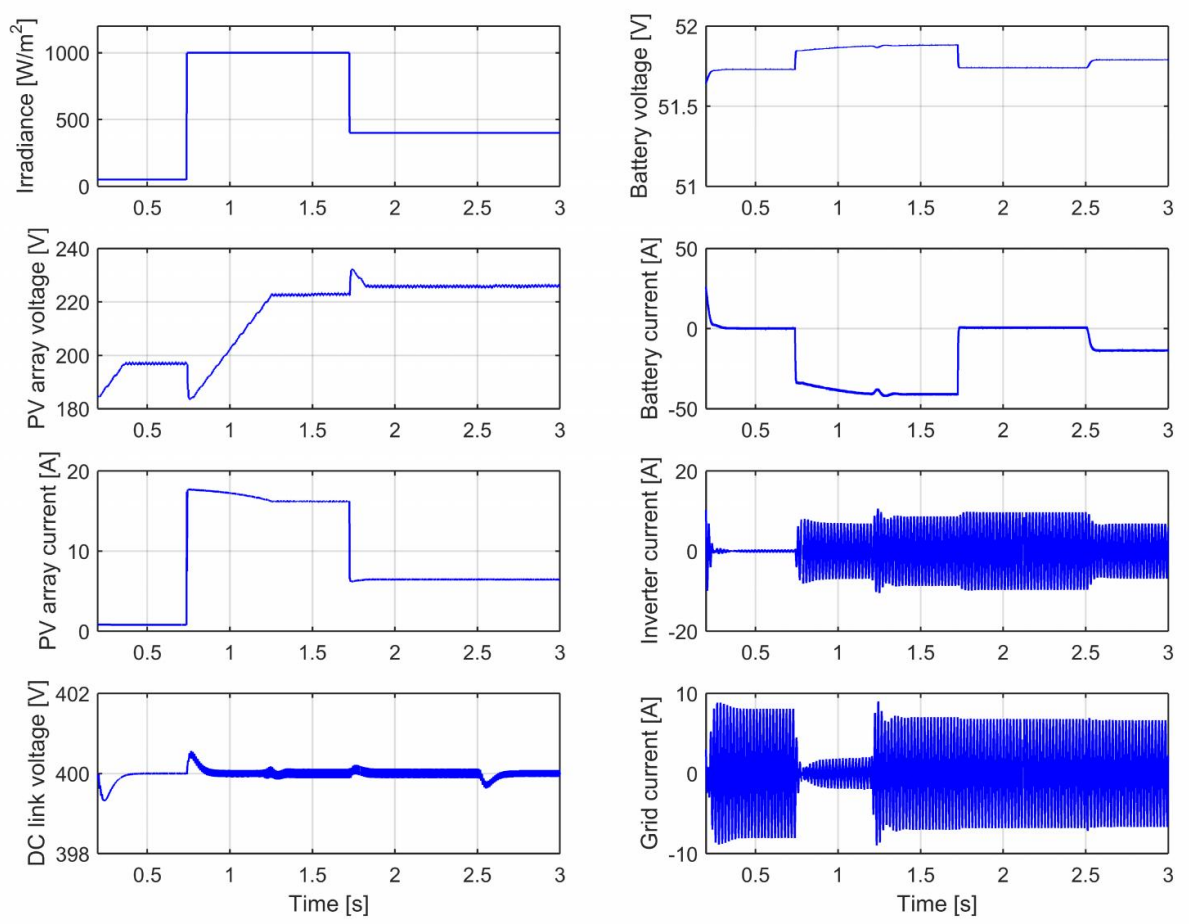

Fig. 8: The changes in voltages and currents at different terminals in the system for step changes in irradiance at $t = [0.75\ 1.75]$ s and load change at $t = 2.5$ s.

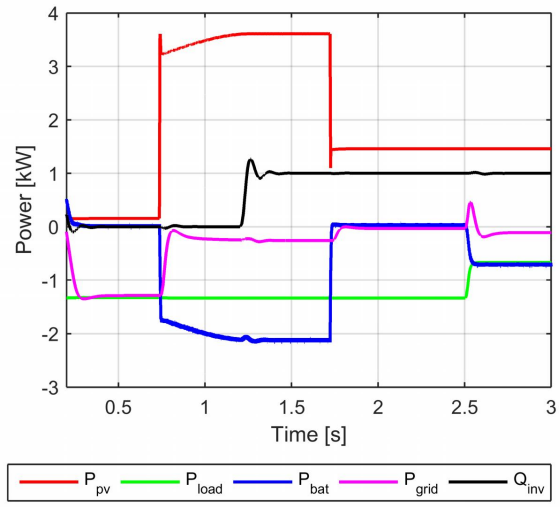

Fig. 9: Power flow between components during normal operation.

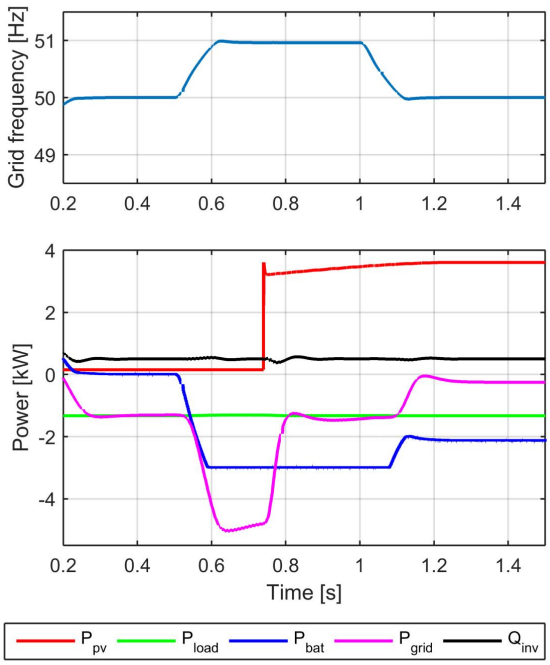

Fig. 10: Power flow between components during grid frequency increase.

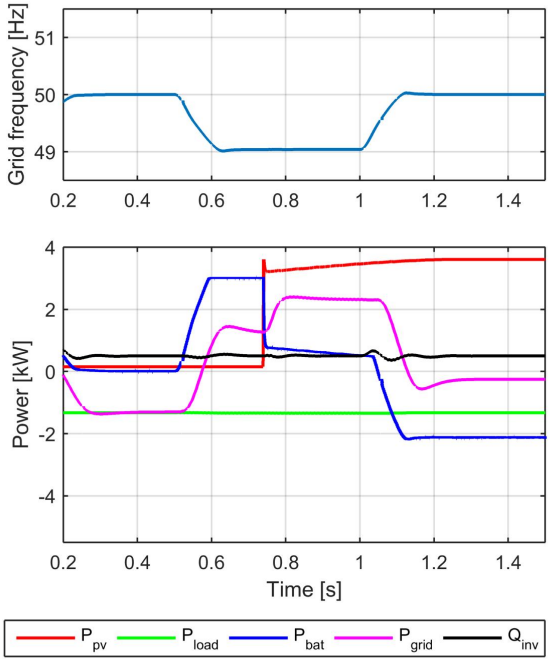

Fig. 11: Power flow between components during grid frequency decrease.